Response of microbial community function to fluctuating geochemical conditions within a legacy radioactive waste trench environment

Xabier Vázquez-Campos[1], Andrew S. Kinsela[2,3], Mark W. Bligh[2,3], Jennifer J. Harrison[3], Timothy E. Payne[3] & T. David Waite[2*]

[1]NSW Systems Biology Initiative, School of Biotechnology and Biomolecular Sciences, The University of New South Wales, Sydney, New South Wales 2052, Australia

[2]UNSW Water Research Centre and School of Civil and Environmental Engineering, The University of New South Wales, Sydney, New South Wales 2052, Australia

[3]Institute for Environmental Research, Australian Nuclear Science and Technology Organisation, Locked Bag 2001, Kirrawee DC, New South Wales 2232, Australia

AEM

(Submitted March 2017)

Conflict of interest: The authors declare no conflict of interest.

*Corresponding author: Professor T.D. Waite; Email: d.waite@unsw.edu.au

Abstract

During the 1960s, small quantities of radioactive materials were co-disposed with chemical waste at the Little Forest Legacy Site (Sydney, Australia) in three metre deep, unlined trenches. Chemical and microbial analyses, including functional and taxonomic information derived from shotgun metagenomics, were collected across a six-week period immediately after a prolonged rainfall event to assess how changing water levels impact upon the microbial ecology and contaminant mobility. Collectively, results demonstrated that oxygen-laden rainwater rapidly altered the redox balance in the trench water, strongly impacting microbial functioning as well as the radiochemistry. Two contaminants of concern, plutonium and americium, were shown to transition from solid-iron-associated species immediately after the initial rainwater pulse, to progressively more soluble moieties as reducing conditions were enhanced. Functional metagenomics revealed the potentially important role that the taxonomically-diverse microbial community played in this transition. In particular, aerobes dominated in the first day followed by an increase of facultative anaerobes/denitrifiers at day four. Towards the mid-end of the sampling period, the functional and taxonomic profiles depicted an anaerobic community distinguished by a higher representation of dissimilatory sulfate reduction and methanogenesis pathways. Our results have important implications to similar near-surface environmental systems in which redox cycling occurs.

Keywords: shotgun metagenomics, radionuclides, plutonium, americium, functional profile.

Introduction

The rapid expansion of an emerging nuclear industry immediately following World War II resulted in substantial volumes of low-level radioactive waste (LLRW) being generated from nuclear fuel cycle, weapons production, medical radioisotope and radiochemical research activities. Although there was no consensus at this time, low-level waste (and in some cases more active material) was commonly disposed of by burial in shallow trenches, as evidenced in the United States at Maxey Flats (1), Oak Ridge (2) and Hanford (3, 4); Canada at Chalk River (5); in the United Kingdom at Harwell (6) and LLRW (7); in Lithuania at Maišiagala (8); and more recently in Ukraine at Chernobyl (9) to name but a few. This was also the case for Australia's only nuclear (research) reactor at Lucas Heights. Known as the Little Forest Legacy Site (LFLS), radioactive materials, including minor amounts of $^{239+240}$Pu and ^{241}Am were placed in narrow (0.6 m), 3 m deep, unlined trenches from 1960 to 1968 (10–12). Large volumes of contaminated non-radioactive materials and equipment were also disposed of in these trenches (10).

The LFLS trenches were constructed in geological matrices exhibiting low hydraulic conductivities to isolate the LLRW from waters associated with the local hydrological cycle (10). However, an unintended consequence of this (also experienced at other disposal sites) has been that periodic intense rainfall and prolonged dry conditions can facilitate complete saturation and desaturation of the more permeable waste material via surface infiltration and evapo(transpi)ration/leakage mechanisms, respectively. This has allowed for redox cycling to occur unabated in the LLRW trenches since their construction, potentially promoting redox tolerant plasticity in the microbial communities present (13).

With actinide mobility, in many instances, strongly dependent on their oxidation state (14), microbial communities can potentially play decisive roles in determining the fate and mobility of such elements in the environment. In general, microbial communities can

influence actinide chemistry by partaking in redox (15–17), dissolution (18, 19), precipitation (20, 21), sorption (22) and/or methylation (23) reactions, which may either enhance or retard contaminant mobility.

Despite this, much of the scientific research to date has focussed on isolated individual species (such as *Geobacter*, *Shewanella* and *Clostridium*) and their impact on actinide, particularly uranium, behaviour. The challenge remains as to how best to identify the role of microorganisms and their functioning within the wider microbial community which may be undergoing external, environmental changes (24). Furthermore, subsurface environments such as aquifers and shallow groundwaters, aside from being poorly studied, have been shown to be havens for microbial novelty not dominated by the well-characterised organisms listed above (25). Culture-independent techniques, such as metagenomics, in which genomic sequences capture the aggregate microbial ecology of a sample (26, 27) have the potential to enhance our understanding of these complex biogeochemical systems.

The question remains at LFLS, and in similar contaminated redox-cycling environments, as to what function microbial communities may be performing in the direct or indirect mobilisation and/or retention of legacy radionuclides. As the establishment of causality between the legacy contaminants and microbial communities cannot be achieved in such a non-invasive environmental study, the aim of this research was to understand the role that periodic inundation from a large rainfall event, and presumably oxygen penetration, had on the concomitant changes to chemistry-radiochemistry and microbial communities in a LLRW trench environment. The two contaminants of major concern, Pu and Am, were the focus of this research with shotgun metagenomics used to examine the microbial systems function and taxonomy.

Materials and methods

Sample collection

Trench water samples were collected on five occasions across a two month period from LFLS, commencing immediately after a substantial rainfall event (days 0, 4, 6, 21 and 47) (Figure S1).

Samples for chemical analyses were collected both with and without an in-line filtration membrane (0.45 µm PES, Waterra FHT-Groundwater). All samples were stored at 4 °C until analysis.

Samples for microbial analyses were collected by directly filtering the trench water using a sterile PES 0.22 µm syringe filter (Sterivex-GP, Merck Millipore). Filters were capped on site before being stored at -18 °C until analysis. Microbial sampling was performed in triplicate to assess inherent variation.

Due to protocols governing sampling at the site, no solid phase material could be extracted from the trenches. All sampling within the trenches pertains to the extraction of soluble or suspended solid-phases from the screened borehole.

Further details are provided in the Supplementary Information.

Chemical analyses of trench waters

The primary radiochemical contaminants, $^{239+240}$Pu and ^{241}Am, were measured by alpha spectroscopy (Canberra). Cations were measured by either ICP-AES or ICP-MS (Thermo) depending on relative concentration. Anions were determined by ion chromatography (Waters). Non-purgeable dissolved organic carbon (0.45 µm filtered) was measured on freshly-collected replicate samples by combustion catalytic oxidation (Shimadzu).

Dissolved ferrous iron (0.45 µm filtered) was preserved in the field with ammonium acetate-buffered phenanthroline solution and measured by spectrophotometry (28).

In field measurements of dissolved sulfide were attempted using methylene blue colorimetry, but were consistently below detection limits (~1 µM) at all sampling time points.

All chemical analyses were performed in triplicate. Further details on the elemental analyses are provided in the Supplementary Information.

DNA extraction and sequencing

The PowerLyzer® PowerSoil® DNA Isolation kit (MO BIO) was used to extract DNA from Sterivex filters following the modified protocol of Jacobs et al (29). Bead beating was performed singularly in a PowerLyzer® 24 Bench Top Bead-Based Homogenizer (MO BIO) at 2000 rpm for 5 min.

Concentration and DNA quality was evaluated with LabChip® GX (PerkinElmer). Libraries were prepared with the TruSeq Nano DNA Library Preparation Kit and sequenced in a NextSeq 500 (Illumina) with a 2×150 bp high output run. Output consisted of paired-end reads with a median insert size of ~480 nt. Reads were deposited at the European Nucleotide Archive (PRJEB14718/ERG009353).

Data processing and functional analyses

Raw sequencing reads were pre-processed with Trim Galore! (http://www.bioinformatics.babraham.ac.uk/projects/trim_galore/) to remove residual adapters as well as short and low quality sequences (Phred33 ≥ 20) while keeping unpaired reads.

Taxonomic profiles were obtained from shotgun metagenomic data by extracting 16S rDNA gene sequences with GraftM v0.10.1 (https://github.com/geronimp/graftM) and mapping them with the 97% clustered GreenGenes database provided by GraftM developers (package 4.39).

Functional analyses of the metagenomic data were performed with HUMAnN2 v0.6.0

(30). Gene families were grouped by MetaCyc reactions (RXN), keeping unmapped and ungrouped reads for calculating copies per million and relative abundances. MetaCyc RXN groups were filtered and only those with at least two replicates from the same sampling time-point with a relative abundance of 10^{-4} or higher were analysed (30). MetaCyc RXN notations have been used as is within Results and Discussion to provide an exact match with the database. RXNs can be considered equivalent to the more traditionally used KO terms from the KEGG database.

Analysis of variance was performed with the software package STAMP v2.1.3 (31) using the Benjamini-Hochberg False Discovery Rate approach (32) for correction of *p*-values.

Results and Discussion

Water level changes and chemical analyses

The initial 220 mm rainfall event resulted in trenches filling to capacity and discharging from the surface or porous near-surface (0–0.2 m) in the 'bathtub' mechanism described by Payne et al (10) (Figure S1). Despite the subsequent 47-day sampling period receiving a further 72 mm of rainfall, which periodically increased trench water levels, an overall decline in trench water levels was observed across the sampling period (Figure S1).

Water quality parameters, including pH, E_h, DO, EC and temperature are provided in Figure 1 and Table 1. Notable observations included an increase in pH (6.30 to 6.60) and a corresponding decrease in E_h (247 to 147 mV) between days 0 and 47.

The concentrations of several elements showed marked changes over time (Figure 2 and Table 1). Iron displayed one of the greatest variations in concentration, increasing from 0.42 mM at day 0, to 1.00 mM by day 47 (Figure 2). The elevated concentrations of iron are unsurprising, given that the LLRW at LFLS was disposed of in-part within ~760 steel drums

(33), and buried within a highly weathered shale geological matrix (11). The continuous presence of Fe(II), even at day 0, confers reducing conditions in excess of E_h values recorded, casting uncertainty over the absolute values supplied by the E_h probe. The increase in Fe(II) concentrations with time was likely due to Fe(III) oxyhydroxide reduction, an observation supported by the concurrent liberation of Si and P, two elements that are typically co-associated with Fe(III)-oxyhydroxide at LFLS (34). The constant concentrations of expected conservative elements Cl^- and K suggest that the drop in trench water level was due to subsurface outflow rather than evaporative processes across the course of sampling. Other important elemental transitions included a 10-fold decrease in dissolved sulfur concentrations (presumed to be sulfate), from an initial concentration of 62.4 to 6.2 µM at day 47 (Figure 2). Nitrate concentrations doubled between days 0 and 6 (from 0.24 to 0.55 µM) after which they decreased to below detection limits at days 21 and 47 (Figure 2).

The total (unfiltered) ^{241}Am activity increased from 15.7 to 27.8 Bq/L (1.8-fold increase) while the soluble (filtered) fraction increased 3.4-times (7.2 to 24.7 Bq/L) between days 0 and 47 (Figure 3). Although the activity of the total $^{239+240}$Pu showed a proportionally smaller increase than ^{241}Am across the sampling period, from 30.4 to 45.6 Bq/L (1.5 times), the soluble fraction increased from 0.21 at Day 0 and reached a maximum of 0.80 (35.1 Bq/L) by day 21. Previous redox state measurements at LFLS found that Pu was present in the Pu(IV) (64.5%) and colloidal/Pu(III) (35.5%) states whilst Am was present exclusively as Am(III) (35). The vast quantities of Fe(II) as well as the results of ancillary measurements (DO, ORP) would suggest that Pu(IV) and Am(III) were again the dominant oxidation states of the trench water contaminants.

Community composition

Community profiles showed that *Bacteria* dominated the trench water microbial community across the entire sampling period. A total of 70 phyla out of the 85 included in the

GreenGenes database were detected at some point and 11 phyla with values over 1% of the total community at all times.

Archaea oscillated between 2.6 and 10.6% of the classified reads with minimum and maximum at days 4 and 47, respectively. *Micrarchaeota* and *Parvarchaeota* were the most abundant phyla at all times with a combined 45.5–55.9% of *Archaea*, while remaining sequences were shared in variable proportions between the TACK superphylum and *Euryarchaeota* (Figure 4). Although the fraction of TACK decreased over time from 24.8% at day 0 to 12.4% at day 47, *Euryarchaeota* reached a maximum at day 47 contributing 37.2% of all *Archaea*. These changes were derived mainly from variations in the SAGMA-X family (*Thaumarchaeota*), related to the ammonia oxidising archaeon '*Ca.* Nitrosotalea' (36, 37) and, in *Bathyarchaeota* (MCG), which includes the only potential non-euryarchaeal methanogens (37, 38) and/or one of the few acetogenic *Archaea* (39). The increase in total *Archaea* abundance over time was related to changes to and ANME-2d, *Methanoregulaceae* and *Methanosaetaceae* families, implicated in methane metabolism (40–42) as well as the *Micrarchaeota* and *Parvarchaeota* phyla.

Only 8 bacterial phyla grouped more than 5% of the total bacterial reads at any one sampling point, and amongst them, only *Chloroflexi*, OD1 (*Parcubacteria*), OP11 (*Microgenomates*), OP3 (*Omnitrophica*) and *Proteobacteria* were within the 10 most abundant bacterial phyla at all times (Figure 4). The principal changes observed over time refer to *Proteobacteria*, TM7 (*Saccharibacteria*), OP3, *Acidobacteria* and OD1. While the proportion of TM7 and *Acidobacteria* decreased from day 0, both OP3, and OD1 reached their maximum by day 47 (18.9% and 14.7%). The *Proteobacteria*, often the most abundant phylum, showed a conspicuous increase, mainly due to *Betaproteobacteria*, comprising 48.7% of all classified reads at day 4. The order *Burkholderiales* was identified as being primarily responsible for this change (42.6% of total), esp. the genus *Ralstonia* (20.3%)

within *Oxalobacteraceae* (34.0%). These bacteria were also responsible for the altered functional profile observed at day 4.

A complete taxonomic profile of all sample replicates at each individual time point is provided in Supplementary Information. An important aside to be noted with this data is the inherent reproducibility between sample triplicates. This finding provides a level of reassurance with regards to the aggregate nature of these water samples, often neglected in similar studies.

Carbon cycling

Initial time points were characterised by a significantly ($p \leq 0.05$) higher relative abundance of RXNs using molecular dioxygen as substrate such as: cytochrome-c oxidase (CYTOCHROME-C-OXIDASE-RXN, EC:1.9.3.1, Figure 5A), quinol–cytochrome-c reductase (1.10.2.2-RXN) and several mono- and dioxygenases. This was combined with a significantly ($p \leq 0.05$) lower relative abundance of methanogenesis-related RXNs, nitrogenase (ferredoxin, NITROGENASE-RXN), rubisco (RIBULOSE-BISPHOSPHATE-CARBOXYLASE-RXN), or heterolactic fermentation (PHOSPHOKETOLASE-RXN). Catalase (CATAL-RXN, EC:1.11.1.6/21, see Reactive oxygen species detoxification in SI) gene relative abundance was highest at day 4 along with several ABC transporters and phosphotransferases, e.g. D-ribopyranose, D-xylose, spermidine or L-arginine, as well as assimilatory sulfur and nitrogen pathway RXNs (refer to SI for details). The higher relative abundances of all these genes at day 4 suggest a metabolism more dependent on oxygen, i.e. aerobic, or at least microaerophilic (see Nitrogen cycling). It also confers a higher dependence on available organic carbon (viz. heterotrophy), or on the presence of decaying complex organic matter (43).

With regard to the latter mechanism, the results suggest that soil particles and

associated organo-chemicals were leached from material above the trenches during and immediately after rainfall. This was evidenced by the increased proportion of soil-associated *Actinobacteria* at day 0, which diminished to 0.71% by day 4 (Figure 4). Furthermore, the presence of genes encoding for enzymes representing chitin degradation, such as chitobiase (RXN-12625, EC:3.2.1.52), diminished progressively until day 47 indicating a potential one-off provision of chitin, matching the leaching hypothesis (Figure S2).

The other primary biopolymer found in soil is cellulose (44). The relative abundance of cellulase (RXN-2043, EC:3.2.1.4) showed no significant differences between days 0, 21 and 47 ($p = 0.172$) suggesting a consistent supply of cellulose (Figure 5B). The exception, noted at day 4, can be explained by the proliferation of *Burkholderiales*. The constant abundance of cellulose is unsurprising given the historical records which indicate a range of organic (particularly cellulose-based) compounds were co-disposed of in the LFLS trenches (11). This hypothesis accords with previous stable isotope measurements, which identified the degradation of legacy organic matter as being responsible for enriched $\delta^{13}C$ (inorganic) values measured near the trench (11).

Lignin is present to a lesser or greater extent in all plant biomass. From the list of enzymes in the literature capable of degrading lignin (45, 46), only below-threshold levels of certain genes were detected: versatile peroxidase (RXN0-267, EC:1.11.1.16), dye peroxidase (RXN-11813, EC:1.11.1.19) and laccase (LACCASE-RXN, EC:1.10.3.2). The overall lack of genes for proteins capable of lignin degradation strengthens the hypothesis that trench waste material is the source of cellulosic material rather than being derived from the degradation of plant material from the topsoil.

The two fundamental genes representing the glyoxylate pathway, isocitrate lyase (ISOCIT-CLEAV-RXN, EC:4.1.3.1, Figure S3) and malate synthase (MALSYN-RXN, EC:4.1.3.2, Figure 5C) showed between 3–4 times higher relative abundance in days 0 and 4

when compared to day 47. This pathway facilitates the use of short chain carbon compounds (C2–C3) for anabolic purposes, compounds especially generated during anaerobic processes. Although the glyoxylate pathway genes have been previously detected in organisms living in anaerobic environments (47), it was absent from strict anaerobic organisms based on the results from EggNOG (48), KEGG (49) and UniProtKB (50) databases (as of 05/05/2016). This finding supports the hypothesis that trench waters became anoxic as the water level declined, promoting conditions which favour the development of strict anaerobes. Furthermore, the aerobic community which developed immediately after the rainfall event likely utilised (and benefited from) the short chain carbon compounds generated by preceding anaerobic conditions.

Both acetoclastic and hydrogenotrophic methanogenesis pathways were evident from the functional profile analysis. Similar maximum relative abundances, about $1.4 \cdot 10^{-4}$, of 5-methyltetrahydrosarcinapterin:corrinoid/iron-sulfur protein *Co*-methyltransferase (RXN-12908, EC:2.1.1.245, Figure 5D) and coenzyme F_{420}-dependent hydrogenase (COENZYME-F420-HYDROGENASE-RXN, EC:1.12.98.1, Figure S4), which are specific RXNs for the methanogenesis from acetate and H_2 and CO_2, were observed at day 47. The presence of methanogenesis-specific RXNs is supported by previous isotopic measurements, showing δ^2H enrichment, relative to $\delta^{18}O$, in the vicinity of the trenches (11). Concurrently, the taxonomy revealed the presence of the ANME-2d division contributing up to 13.8% of all *Archaea* at day 47 (1.5% of the community). The ANME-2d division was initially linked to the anaerobic oxidation of methane using nitrate (40) or even nitrite (51), constituting one of the primary methane sinks in anaerobic conditions. However, recent research has shown that some of the members of this taxa are able utilise Fe(III) in place of NO_2^- / NO_3^- (42, 52, 53). This provides a more reasonable explanation given the limited nitrate present and abundance of Fe during the later sampling days.

Sulfur cycling

The relative abundance of sulfite cytochrome *c* reductase (SULFITE-DEHYDROGENASE-RXN, EC:1.8.2.1, Figure S5), involved in the assimilatory reduction of sulfate, peaked at day 4, with ~10 times higher relative abundance compared to day 0. At the same time, dissimilatory sulfate reduction RXNs, e.g. dissimilatory sulfite reductase (HYDROGENSULFITE-REDUCTASE-RXN, EC:1.8.99.3), followed the opposite trend, with a maximum at day 47 (Figure 5E). The combined relative abundance of all the putative sulfate reducing bacteria (SRB) taxa detected (mainly *Syntrophobacterales*, *Thermodesulfovibrionaceae* and *Desulfobacterales*) also increased over time, from 2.3% of the total prokaryotes at day 0 to 4.9% at day 47. Dissimilatory sulfate reduction is one of the major redox processes in both natural (54) and artificial (55) anaerobic environments. The ten-fold reduction in the sulfur concentration is thought to result from the loss of dissolved sulfate via reduction to sulfide and subsequent precipitation of insoluble heavy metal sulfides, particularly FeS. This interpretation is supported by previous reports of sulfate reduction based on isotopic fractionation and severe (10 to 100-fold) depletion in sulfate concentrations in trench waters relative to surrounding wells (11). The potential contribution of sulfate- and nitrite-dependent anaerobic methane oxidation (S-DAMO and N-DAMO respectively) was discounted due to the near complete absence of ANME taxa (*Archaea*) aside from ANME-2d, and NC10 (*Bacteria*) (see Nitrogen cycling) (42, 51, 56, 57).

Nitrogen cycling

The (inorganic) nitrogen cycle was mostly represented by RXNs related to denitrification and assimilatory nitrogen reactions (Figure S6) though nitrogen fixation (NITROGENASE-RXN, EC:1.18.6.1) was the most predominant N-associated RXN. All other prominent N-associated RXNs peaked at day 4 with the exception of hydroxylamine reductase (HYDROXYLAMINE-REDUCTASE-RXN, EC:1.7.99.1) and ammonia

oxygenase (AMONITRO-RXN, EC:1.14.99.39). The increase in nitrate concentrations observed between days 4 and 6 (0.236 and 0.552 µM respectively) might be derived from the oxidation of NO by nitric oxide dioxygenase (R621-RXN, EC:1.14.12.17). This surge in the relative abundance of nitrogen metabolism RXNs (at day 4) coincided with an increased dominance of *Betaproteobacteria*, mostly *Burkholderiales*. *Betaproteobacteria* have been linked to denitrification processes in a uranium-polluted aquifer in Rifle (USA) (58) and they may play a similar ecological role at LFLS. However, the increase in nitrate concentrations could equally be indicative of NO or NO_2^- oxidation, originally produced by the aerobic oxidation of ammonium by the *Thaumarchaeota* (59, 60).

The inorganic nitrogen cycling results provide important information regarding the transition from aerobic to anaerobic conditions as the water level declines. The competing requirements of nitrate respiration, which necessitates oxygen-limiting conditions at a minimum (61), and NO dioxygenase needing molecular oxygen, collectively suggest that at day 4 the trench waters were no longer aerobic, but more likely microaerophilic/hypoxic. However, many facultative anaerobes are capable of using nitrate as an alternate electron acceptor when oxygen is not available. As such, the high relative abundance of nitrate reducing enzyme genes at day 4 could be a confounding effect associated with the increased abundance of *Burkholderiales*. This was confirmed by searching the denitrifying pathway in KEGG (map00910) (as of 08/07/2016) (49).

Iron cycling

Temporal increases in Fe(II) concentrations may be associated with the use of Fe(III) during anaerobic respiration, previously attributed to decaheme *c*-type cytochromes from the OmcA/MtrC family present in iron-reducing bacteria (FeRB) such as *Shewanella* spp. and *Geobacter* spp. (62, 63). However, their representation in the trench water metagenome data was scarce (relative abundance $\leq 10^{-6}$). It is known that for respiration to occur, FeRB often

require direct physical contact with Fe(III) solids (64). As only aqueous/suspended phase sampling was permissible at LFLS, it is possible the under representation of a FeRB community was due to a sampling regime in which the solid-phase is largely excluded.

However, the genes associated with RXNs specific to the Fe(II) oxidation pathway (via rusticyanin, PWY-6692): ubiquinone-cytochrome-*bc1* reductase (EC:1.10.2.2, RXN-15829) and *aa3*-type cytochrome oxidase (EC:1.9.3.1, RXN-15830) were present, despite no RXNs with rusticyanin as either product or substrate being identified. The presence of both RXNs could be because HUMAnN2 could not distinguish between the 'generic' quinol–cytochrome-c reductase (RXN-15816, EC:1.10.2.2), and cytochrome *c* oxidase (CYTOCHROME-C-OXIDASE-RXN) respectively, particularly when analysing short reads.

Previous research on soils experiencing fluctuating redox conditions and active iron cycling have shown they frequently lack 'typical' Fe(III)-respiring bacteria (65), being outcompeted by sulfate respiration (66). Despite Fe(III) being a more thermodynamically favourable electron acceptor it is commonly acknowledged that sulfate respiration often outcompetes Fe(III) respiration in both high and low sulfate environments (66, 67). High levels of sulfate reduction in low-sulfate environments, akin to the LFLS trenches, has been previously observed to occur in the presence of crystalline Fe(III) oxyhydroxides that partially re-oxidise sulfide generated by SRB to elemental sulfur (67). This mechanism provides a plausible explanation for our observations at LFLS. The large concentration of dissolved Fe(II) in the trench waters would likely contribute to the Fe(II)-catalysed transformation of amorphous ferrihydrite to more crystalline, thermodynamically-favourable forms (68, 69), although this would be limited to some extent by the large concentrations of dissolved organic matter and silica (70). Furthermore, the abiotic reduction of crystalline Fe(III) oxyhydroxides would severely limit the energy acquisition by FeRB and therefore the FeRB would only outcompete SRB when sulfate and other reducible sulfur compounds were

totally consumed.

Alternatively, fermentative bacteria such as *Propionibacterium freudenreichii* have previously been observed to reduce Fe(III) by using humic substances as an electron mediator (71). Both heterolactic and propionic acid fermentation pathways showed high relative abundances based on phosphoketolase (PHOSPHOKETOLASE-RXN, EC:4.1.2.9) and methylmalonyl-CoA decarboxylase (RXN0-310, EC:4.1.1.41), respectively (Figure S7). Their decrease in relative abundance (at day 4) could be explained by the lack of fermentative pathways present in the genomes associated with the population shift, i.e. increase in *Burkholderiales*. This was confirmed by searching (as of 08/06/2016) methylmalonyl-CoA decarboxylase and phosphoketolase in the KEGG maps (map00640 and map00030, respectively).

To add further complexity, waste disposal records from LFLS indicate that numerous steel drums (~760) were co-disposed of in the trenches (33). Based on the active sulfate respiration observed in the trench waters, we would expect that iron/steel materials may have suffered microbially induced corrosion (MIC) (72), potentially contributing to the elevated Fe(II) concentrations. However, the main Fe MIC product is likely FeS (72), which can be utilised by *Gallionella ferruginea*, an iron oxidising bacteria (FeOB) (73). The presence of 1.9% of *Gallionellaceae* (over the total community composition) at day 0 and 2.9% of *Crenothrix*, a non-FeOB usually associated with Fe-mineralising biofilms (74), would suggest the existence of transient microaerophilic iron oxidising activity in the trench water. Furthermore, this process would also provide an explanation for a persistent source of Fe(III) (oxy)hydroxides and their ongoing interaction with the S-cycle.

Synthesis of trench processes and radiochemical mobilisation implications

The biogeochemistry of this dynamic system is conceptually described by the elemental

cycling schematic shown in Figure 6. Immediately following the rainfall event, the E_h reached its most oxidising value (247 mV) with the microbial community characterised by higher relative abundances of pathways related to aerobic (or at least microaerophilic) heterotrophic metabolism and one capable of chitin degradation. Although conditions were not strongly oxidising, this pulse of oxic water would be sufficient to induce the abiotic oxidation of part of the large store of dissolved Fe(II), likely forming a combination of the reactive Fe(III) oxyhydroxides ferrihydrite and silica-ferrihydrite, along with the more crystalline oxyhydroxide lepidocrocite, as has previously been observed in these trench waters (34). As both Am(III) and Pu(III)/(IV) are known to strongly sorb to sediments and iron oxides (14), it is of little surprise to observe the greatest proportions of (suspended) solid-associated actinides at this time point (day 0, Figure 3). Note that even though the majority of Am (54.3%) and particularly Pu (78.8%) were associated with a solid-fraction >0.45 µm, they were still extracted from the trench under our low-flow sampling method. This finding implies that colloid-associated Pu, and to a lesser extent Am, remains mobile within the trench waters, congruent with observations from other legacy radioactive waste sites (75). Interestingly though, the Pu migration distance away from source at LFLS in groundwater has been shown to be much smaller (~1 order of magnitude less) compared to other legacy locations such as the Nevada Test Site (76), Rocky Flats (77) and Mayak (78). We attribute this to a low permeability soil matrix, inhibiting downward migration to the connected/permanent water table, coupled with the biogeochemical conditions within the trenches themselves. The high concentrations of Fe(II), circumneutral pH and proliferation of aerobic heterotrophs drives the rapid formation of large quantities of Fe(III) oxides. The quantity of Fe(III) oxides that form upon oxic rainwater intrusion is evidently sufficient to contain the bulk of contaminants within the trenches during ‘bathtub’ overflow events. The rate of Fe(II) oxidation is likely to be crucial for the ongoing attenuation of Pu and Am at

LFLS (34).

By day 4, as water levels rapidly decrease, an increase of *Burkholderiales* (*Betaproteobacteria*) generates a functional profile disturbance and, while the aerobic profile is maintained, it is also the time-point at which nitrogen cycling (e.g. nitrate respiration) becomes most active (Figure 6;). Therefore, day 4 represents a potential transition away from oxic conditions derived from rain infiltration, though this sequence of events is somewhat confounded by the microbial growth lag phase associated with aerobic respirators.

Over the following weeks (days 21 and 47), the microbial community transitions to a functional profile dominated by carbon fixation, methanogenesis and sulfate respiration pathways (Figure 6;). The increase in anaerobicity correlated with increasing concentrations of soluble Fe and soluble radionuclides and a depletion of sulfate and nitrate. In the case of Am, although the total activity increased gradually as the water level in the trench declined, the soluble fraction increased by a greater proportion (Figure 3). This indicates that either a desorption or dissolution process occurred. Such an increase in the Am soluble fraction can likely be accounted for by the reductive dissolution of Fe(III) oxyhydroxides.

The Pu behaviour in the trenches presents a more complex temporal dynamic due, in part, to its more varied redox chemistry. As conditions become more reducing over time, one would expect to observe soluble Pu activities increase, through both the dissolution of Fe(III) oxides and, to a lesser extent, from Pu(IV) to Pu(III) reduction. In an interesting point of difference to Am, our results show that Pu proportionally remained in the particle-associated fraction for a substantially longer period, even as the dissolved Am(III) activity and Fe(II) concentration increased. The reason for the differing solution/solid-phase partitioning observed for Pu and Am is not clear based on the evidence to hand. Indeed, the inability to sample solid materials from within the trenches has limited more conclusive understanding.

However, we suggest the differing Am and Pu associations are likely due to different redox states, based on the previous measurements at LFLS, which showed a dominant Pu oxidation state of +4 (35). Electrostatically, Pu(IV), as the neutral hydrolysed cation $Pu(OH)_4(aq)$ or as an intrinsic colloid, is more likely sorbed or incorporated into positively charged pseudo-colloids such as Fe(III) oxides, compared to Am^{3+}. This is supported by research showing the highly reversible nature of Am(III) sorption onto poor crystalline iron colloids (79) and association with carbonate- and exchangeable sites on clays (80).

Conclusions

The inability to comprehensively access and sample within legacy radioactive waste environments hampers our ability to comprehend co-occurring elemental cycling and microbial metabolism, potentially curtailing our ability to effectively manage and remediate such sites. The trench-sampling point at LFLS is therefore a particularly useful resource for such research. In this study, our coupled use of metagenomics and chemical analyses has provided a previously unattainable level of understanding for the LFLS trench water, highlighting the responsiveness of the microbial community to external changes and dynamic nature of the resulting chemistry. The combined results show that the trench waters contain a taxonomically diverse microbial community, which has likely evolved in response to variations in energy sources supplied by frequent redox fluctuations. When combined with the complex nature of the waste-form, a myriad of micro-environments has developed within the trenches, allowing for simultaneous O, N, Fe, S and C elemental cycling, as shown by co-occurring metabolic reactions in the aggregate water samples. Consequently, it can be inferred that Pu and Am are subject to persistent reducing conditions (as evident from active iron oxide dissolution, sulfate reduction and methanogenesis) when the water level is low between rainfall events. These reductive processes maintain Pu and Am solubility, despite the

occasional onset of oxidising conditions associated with rainfall events. Ultimately however, the high concentrations of Fe present and the tendency of Fe(II) to be relatively rapidly oxidised to strongly sorbing Fe(III) (oxy)hydroxide solids on exposure to oxic conditions results in limited transport of Pu and Am.

Although the findings described above are intrinsically linked to the specific site under investigation, they provide important generic insights into the dynamic biogeochemical behaviour of iron-rich, redox-cycling environments. Of particular interest is the rapid response of the microbial community to dynamic redox conditions and the potential impact upon persistent contaminant solubility and enhanced mobility.

Acknowledgements

ANSTO staff members are thanked for their valuable contributions: Kerry Wilsher (fieldwork, laboratory analyses), Sangeeth Thiruvoth (actinides), Brett Rowling (fieldwork, inorganics), Henri Wong (inorganics), Chris Vardanega (inorganics) and Dioni Cendón (discussion). The Australian Bureau of Meteorology is acknowledged for rainfall data.

Author contribution

Study concept and experimental design: XVC, ASK, TDW. Fieldwork: ASK. Chemical and radiochemical analyses: ASK, JJH. Molecular biology and bioinformatics analyses: XVC. Contribution of reagents/materials/analysis tools: TEP, TDW. Manuscript writing: XVC, ASK. Revision and review of the manuscript: XVC, ASK, MWB, TDW.

References

1. Cleveland JM, Rees TF. 1981. Characterization of plutonium in Maxey Flats radioactive trench leachates. Science 212:1506–1509.

2. Saunders JA, Toran LE. 1995. Modeling of radionuclide and heavy metal sorption around low- and high-pH waste disposal sites at Oak Ridge, Tennessee. Appl Geochem 10:673–684.

3. Cantrell KJ, Felmy AR. 2012. Plutonium and americium geochemistry at Hanford: a site-wide review. RPT-DVZ-AFRI-001 PNNL-21651. Pacific Northwest National Laboratory, Washington (USA).

4. Gerber MS. 1992. Past practices technical characterization study — 300 area — Hanford site. WHC-MR-0388. UC-702. Westinghouse Hanford Company, Richland, WA.

5. Killey RWD, Rao RR, Eyvindson S. 1998. Radiocarbon speciation and distribution in an aquifer plume and groundwater discharge area, Chalk River, Ontario. Appl Geochem 13:3–16.

6. Fellingham L, Graham A, Stiff S. 2003. Characterisation and remediation of beryllium waste pits in the Southern storage area at Harwell, p. 1041–1049. *In* ASME 2003 9th International Conference on Radioactive Waste Management and Environmental Remediation. American Society of Mechanical Engineers, Oxford, England.

7. Wilkins MJ, Livens FR, Vaughan DJ, Lloyd JR, Beadle I, Small JS. 2010. Fe(III) reduction in the subsurface at a low-level radioactive waste disposal site. Geomicrobiol J 27:231–239.

8. Gudelis A, Gvozdaitė R, Kubarevičienė V, Druteikienė R, Lukoševičius Š, Šutas A. 2010. On radiocarbon and plutonium leakage to groundwater in the vicinity of a shallow-land radioactive waste repository. J Environ Radioact 101:443–445.

9. Bugai D, Kashparov V, Dewiére L, Khomutinin Y, Levchuk S, Yoschenko V. 2005. Characterization of subsurface geometry and radioactivity distribution in the trench containing Chernobyl clean-up wastes. Environ Geol 47:869–881.

10. Payne TE, Harrison JJ, Hughes CE, Johansen MP, Thiruvoth S, Wilsher KL, Cendón DI, Hankin SI, Rowling B, Zawadzki A. 2013. Trench “bathtubbing” and surface plutonium contamination at a legacy radioactive waste site. Environ Sci Technol 47:13284–13293.

11. Cendón DI, Hughes CE, Harrison JJ, Hankin SI, Johansen MP, Payne TE, Wong H, Rowling B, Vine M, Wilsher K, Guinea A, Thiruvoth S. 2015. Identification of sources and processes in a low-level radioactive waste site adjacent to landfills: groundwater hydrogeochemistry and isotopes. Aust J Earth Sci 62:123–141.

12. Hughes CE, Cendón DI, Harrison JJ, Hankin SI, Johansen MP, Payne TE, Vine M, Collins RN, Hoffmann EL, Loosz T. 2011. Movement of a tritium plume in shallow groundwater at a legacy low-level radioactive waste disposal site in eastern Australia. J Environ Radioact 102:943–952.

13. Pett-Ridge J, Firestone MK. 2005. Redox fluctuation structures microbial communities in a wet tropical soil. Appl Environ Microbiol 71:6998–7007.

14. Choppin GR. 2007. Actinide speciation in the environment. J Radioanal Nucl Chem 273:695–703.

15. Kimber RL, Boothman C, Purdie P, Livens FR, Lloyd JR. 2012. Biogeochemical behaviour of plutonium during anoxic biostimulation of contaminated sediments. Mineral Mag 76:567–578.

16. Lloyd JR, Sole VA, Praagh CVGV, Lovley DR. 2000. Direct and Fe(II)-mediated reduction of technetium by Fe(III)-reducing bacteria. Appl Environ Microbiol 66:3743–3749.

17. Renshaw JC, Butchins LJC, Livens FR, May I, Charnock JM, Lloyd JR. 2005. Bioreduction of uranium: Environmental implications of a pentavalent intermediate. Environ Sci Technol 39:5657–5660.

18. Francis AJ, Dodge CJ, Gillow JB. 2008. Reductive dissolution of Pu(IV) by *Clostridium* sp. under anaerobic conditions. Environ Sci Technol 42:2355–2360.

19. Renshaw JC, Law N, Geissler A, Livens FR, Lloyd JR. 2009. Impact of the Fe(III)-reducing bacteria *Geobacter sulfurreducens* and *Shewanella oneidensis* on the speciation of plutonium. Biogeochemistry 94:191–196.

20. Fomina M, Charnock JM, Hillier S, Alvarez R, Gadd GM. 2007. Fungal transformations of uranium oxides. Environ Microbiol 9:1696–1710.

21. Wilkins MJ, Livens FR, Vaughan DJ, Beadle I, Lloyd JR. 2007. The influence of microbial redox cycling on radionuclide mobility in the subsurface at a low-level radioactive waste storage site. Geobiology 5:293–301.

22. Vázquez-Campos X, Kinsela AS, Collins RN, Neilan BA, Aoyagi N, Waite TD. 2015. Uranium binding mechanisms of the acid-tolerant fungus *Coniochaeta fodinicola*. Environ Sci Technol 49:8487–8496.

23. Amachi S, Fujii T, Shinoyama H, Muramatsu Y. 2005. Microbial influences on the mobility and transformation of radioactive iodine in the environment. J Nucl Radiochem Sci 6:21–24.

24. Bertin PN, Heinrich-Salmeron A, Pelletier E, Goulhen-Chollet F, Arsène-Ploetze F, Gallien S, Lauga B, Casiot C, Calteau A, Vallenet D, Bonnefoy V, Bruneel O, Chane-Woon-Ming B, Cleiss-Arnold J, Duran R, Elbaz-Poulichet F, Fonknechten N, Giloteaux L, Halter D, Koechler S, Marchal M, Mornico D, Schaeffer C, Smith AAT, Van Dorsselaer A, Weissenbach J, Médigue C, Le Paslier D. 2011. Metabolic diversity among main microorganisms inside an arsenic-rich ecosystem revealed by meta- and proteo-genomics. ISME J 5:1735–1747.

25. Castelle CJ, Hug LA, Wrighton KC, Thomas BC, Williams KH, Wu D, Tringe SG, Singer SW, Eisen JA, Banfield JF. 2013. Extraordinary phylogenetic diversity and metabolic versatility in aquifer sediment. Nat Commun 4:2120.

26. Aguiar-Pulido V, Huang W, Suarez-Ulloa V, Cickovski T, Mathee K, Narasimhan G. 2016. Metagenomics, metatranscriptomics, and metabolomics approaches for microbiome analysis. Evol Bioinform 5.

27. Allen EE, Banfield JF. 2005. Community genomics in microbial ecology and evolution. Nat Rev Micro 3:489–498.

28. APHA, AWWA, WEF. 1998. Standard methods for the examination of water and wastewater20th ed. APHA-AWWA-WEF, Washington, D.C.

29. Jacobs J, Rhodes M, Sturgis B, Wood B. 2009. Influence of environmental gradients on the abundance and distribution of *Mycobacterium* spp. in a coastal lagoon estuary. Appl Environ Microbiol 75:7378–7384.

30. Abubucker S, Segata N, Goll J, Schubert AM, Izard J, Cantarel BL, Rodriguez-Mueller B, Zucker J, Thiagarajan M, Henrissat B, White O, Kelley ST, Methé B, Schloss PD, Gevers D, Mitreva M, Huttenhower C. 2012. Metabolic reconstruction for metagenomic data and its application to the human microbiome. PLoS Comput Biol 8:e1002358.

31. Parks DH, Tyson GW, Hugenholtz P, Beiko RG. 2014. STAMP: statistical analysis of taxonomic and functional profiles. Bioinformatics 30:3123–3124.

32. Benjamini Y, Hochberg Y. 1995. Controlling the False Discovery Rate: A Practical and Powerful Approach to Multiple Testing. J Roy Stat Soc B 57:289–300.

33. Payne TE. 2012. Background report on the Little Forest Burial Ground legacy waste site. ANSTO / E-780. Institute for Environmental Research, Australian Nuclear Science and Technology Organisation, Lucas Heights, N.S.W. (AU).

34. Kinsela AS, Jones AJ, Bligh MW, Pham AN, Collins RN, Harrison JJ, Wilsher KL, Payne TE, Waite TD. 2016. Influence of dissolved silicate on Fe(II) oxidation. Environ Sci Technol 50:11663–11671.

35. Ikeda-Ohno A, Harrison JJ, Thiruvoth S, Wilsher K, Wong HKY, Johansen MP, Waite TD, Payne TE. 2014. Solution speciation of plutonium and americium at an Australian legacy radioactive waste disposal site. Environ Sci Technol 48:10045–10053.

36. Jiang L, Zheng Y, Chen J, Xiao X, Wang F. 2011. Stratification of archaeal communities in shallow sediments of the Pearl River Estuary, Southern China. Antonie van Leeuwenhoek 99:739–751.

37. Meng J, Xu J, Qin D, He Y, Xiao X, Wang F. 2014. Genetic and functional properties of uncultivated MCG archaea assessed by metagenome and gene expression analyses. ISME J 8:650–659.

38. Evans PN, Parks DH, Chadwick GL, Robbins SJ, Orphan VJ, Golding SD, Tyson GW. 2015. Methane metabolism in the archaeal phylum Bathyarchaeota revealed by genome-centric metagenomics. Science 350:434–438.

39. He Y, Li M, Perumal V, Feng X, Fang J, Xie J, Sievert SM, Wang F. 2016. Genomic and enzymatic evidence for acetogenesis among multiple lineages of the archaeal phylum Bathyarchaeota widespread in marine sediments. Nat Microbiol 16035.

40. Haroon MF, Hu S, Shi Y, Imelfort M, Keller J, Hugenholtz P, Yuan Z, Tyson GW. 2013. Anaerobic oxidation of methane coupled to nitrate reduction in a novel archaeal lineage. Nature 500:567–570.

41. Karakashev D, Batstone DJ, Trably E, Angelidaki I. 2006. Acetate oxidation is the dominant methanogenic pathway from acetate in the absence of methanosaetaceae. Appl Environ Microbiol 72:5138–5141.

42. Leu A, Hu S, Cai C, Yuan Z, Orphan VJ, Tyson GW. 2016. Understanding the metabolic potential of ANME-2d and its role in anaerobic methane oxidation coupled to metal reduction. Montreal, Canada.

43. Peng R-H, Xiong A-S, Xue Y, Fu X-Y, Gao F, Zhao W, Tian Y-S, Yao Q-H. 2008. Microbial biodegradation of polyaromatic hydrocarbons. FEMS Microbiol Rev 32:927–955.

44. Beier S, Bertilsson S. 2013. Bacterial chitin degradation—mechanisms and ecophysiological strategies. Front Microbiol 4:149.

45. de Gonzalo G, Colpa DI, Habib MHM, Fraaije MW. 2016. Bacterial enzymes involved in lignin degradation. J Biotechnol 236:110–119.

46. Pollegioni L, Tonin F, Rosini E. 2015. Lignin-degrading enzymes. FEBS J 282:1190–1213.

47. Burow LC, Mabbett AN, Blackall LL. 2008. Anaerobic glyoxylate cycle activity during simultaneous utilization of glycogen and acetate in uncultured *Accumulibacter* enriched in enhanced biological phosphorus removal communities. ISME J 2:1040–1051.

48. Huerta-Cepas J, Szklarczyk D, Forslund K, Cook H, Heller D, Walter MC, Rattei T, Mende DR, Sunagawa S, Kuhn M, Jensen LJ, von Mering C, Bork P. 2016. eggNOG 4.5: a hierarchical orthology framework with improved functional annotations for eukaryotic, prokaryotic and viral sequences. Nucl Acids Res 44:D286–D293.

49. Kanehisa M, Sato Y, Kawashima M, Furumichi M, Tanabe M. 2016. KEGG as a reference resource for gene and protein annotation. Nucl Acids Res 44:D457–D462.

50. Magrane M, Uniprot Consortium. 2011. UniProt Knowledgebase: a hub of integrated protein data. Database 2011:bar009.

51. Cui M, Ma A, Qi H, Zhuang X, Zhuang G. 2015. Anaerobic oxidation of methane: an “active” microbial process. MicrobiologyOpen 4:1–11.

52. Timmers PHA, Welte CU, Koehorst JJ, Plugge CM, Jetten MSM, Stams AJM. 2017. Reverse methanogenesis and respiration in methanotrophic Archaea. Archaea 2017:e1654237.

53. Ettwig KF, Zhu B, Speth D, Keltjens JT, Jetten MSM, Kartal B. 2016. Archaea catalyze iron-dependent anaerobic oxidation of methane. PNAS 113:12792–12796.

54. Grein F, Ramos AR, Venceslau SS, Pereira IAC. 2013. Unifying concepts in anaerobic respiration: Insights from dissimilatory sulfur metabolism. Biochim Biophys Acta Bioenerg 1827:145–160.

55. Paulo LM, Stams AJM, Sousa DZ. 2015. Methanogens, sulphate and heavy metals: a complex system. Rev Environ Sci Biotechnol 14:537–553.

56. Scheller S, Yu H, Chadwick GL, McGlynn SE, Orphan VJ. 2016. Artificial electron acceptors decouple archaeal methane oxidation from sulfate reduction. Science 351:703–707.

57. He Z, Cai C, Wang J, Xu X, Zheng P, Jetten MSM, Hu B. 2016. A novel denitrifying methanotroph of the NC10 phylum and its microcolony. Sci Rep 6:32241.

58. Wrighton KC, Castelle CJ, Wilkins MJ, Hug LA, Sharon I, Thomas BC, Handley KM, Mullin SW, Nicora CD, Singh A, Lipton MS, Long PE, Williams KH, Banfield JF. 2014. Metabolic interdependencies

between phylogenetically novel fermenters and respiratory organisms in an unconfined aquifer. ISME J 8:1452–1463.

59. Könneke M, Schubert DM, Brown PC, Hügler M, Standfest S, Schwander T, Borzyskowski LS von, Erb TJ, Stahl DA, Berg IA. 2014. Ammonia-oxidizing archaea use the most energy-efficient aerobic pathway for CO_2 fixation. PNAS 111:8239–8244.

60. Pester M, Schleper C, Wagner M. 2011. The Thaumarchaeota: an emerging view of their phylogeny and ecophysiology. Curr Opin Microbiol 14:300–306.

61. Fischer M, Falke D, Pawlik T, Sawers RG. 2014. Oxygen-dependent control of respiratory nitrate reduction in mycelium of *Streptomyces coelicolor* A3(2). J Bacteriol 196:4152–4162.

62. Blöthe M, Roden EE. 2009. Microbial iron redox cycling in a circumneutral-pH groundwater seep. Appl Environ Microbiol 75:468–473.

63. Lovley DR, Holmes DE, Nevin KP. 2004. Dissimilatory Fe(III) and Mn(IV) reduction. Adv Microb Physiol 49:219–286.

64. Weber KA, Achenbach LA, Coates JD. 2006. Microorganisms pumping iron: anaerobic microbial iron oxidation and reduction. Nat Rev Micro 4:752–764.

65. DeAngelis KM, Silver WL, Thompson AW, Firestone MK. 2010. Microbial communities acclimate to recurring changes in soil redox potential status. Environ Microbiol 12:3137–3149.

66. Cozzarelli IM, Weiss JV. 2007. Biogeochemistry of Aquifer Systems, p. 843–859. *In* Hurst, CJ, Crawford, RL, Garland, JL, Lipson, DA, Mills, AL, Stetzenbach, LD (eds.), Manual of environmental microbiology. American Society of Microbiology.

67. Hansel CM, Lentini CJ, Tang Y, Johnston DT, Wankel SD, Jardine PM. 2015. Dominance of sulfur-fueled iron oxide reduction in low-sulfate freshwater sediments. ISME J 9:2400–2412.

68. Boland DD, Collins RN, Miller CJ, Glover CJ, Waite TD. 2014. Effect of solution and solid-phase conditions on the Fe(II)-accelerated transformation of ferrihydrite to lepidocrocite and goethite. Environ Sci Technol 48:5477–5485.

69. Pedersen HD, Postma D, Jakobsen R, Larsen O. 2005. Fast transformation of iron oxyhydroxides by the catalytic action of aqueous Fe(II). Geochim Cosmochim Acta 69:3967–3977.

70. Jones AM, Collins RN, Rose J, Waite TD. 2009. The effect of silica and natural organic matter on the Fe(II)-catalysed transformation and reactivity of Fe(III) minerals. Geochim Cosmochim Acta 73:4409–4422.

71. Benz M, Schink B, Brune A. 1998. Humic acid reduction by *Propionibacterium freudenreichii* and other fermenting bacteria. Appl Environ Microbiol 64:4507–4512.

72. Anandkumar B, George RP, Maruthamuthu S, Parvathavarthini N, Mudali UK. 2016. Corrosion characteristics of sulfate-reducing bacteria (SRB) and the role of molecular biology in SRB studies: an overview. Corrosion Rev 34:41–63.

73. Lütters-Czekalla S. 1990. Lithoautotrophic growth of the iron bacterium *Gallionella ferruginea* with thiosulfate or sulfide as energy source. Arch Microbiol 154:417–421.

74. Emerson D, Fleming EJ, McBeth JM. 2010. Iron-oxidizing bacteria: an environmental and genomic perspective. Ann Rev Microbiol 64:561–583.

75. Kersting AB. 2013. Plutonium transport in the environment. Inorg Chem 52:3533–3546.

76. Kersting AB, Efurd DW, Finnegan DL, Rokop DJ, Smith DK, Thompson JL. 1999. Migration of plutonium in ground water at the Nevada Test Site. Nature 397:56–59.

77. Santschi PH, Roberts KA, Guo L. 2002. Organic nature of colloidal actinides transported in surface water environments. Environ Sci Technol 36:3711–3719.

78. Novikov AP, Kalmykov SN, Utsunomiya S, Ewing RC, Horreard F, Merkulov A, Clark SB, Tkachev VV, Myasoedov BF. 2006. Colloid transport of plutonium in the far-field of the Mayak Production Association, Russia. Science 314:638–641.

79. Schäfer T, Artinger R, Dardenne K, Bauer A, Schuessler W, Kim JI. 2003. Colloid-borne americium migration in Gorleben groundwater: Significance of iron secondary phase transformation. Environ Sci Technol 37:1528–1534.

80. Lujanienė G, Beneš P, Štamberg K, Ščiglo T. 2012. Kinetics of plutonium and americium sorption to natural clay. J Environ Radioact 108:41–49.

Table 1. Geochemical parameters measured in the trench water.

Sampling day[a]		0	4	6	21	47	Maximum background concentration[b]
Date		23-Apr	27-Apr	29-Apr	14-May	9-Jun	
Field Parameters	**pH**	6.3	6.22	6.35	6.5	6.6	NA
	E_h (mV)[c]	247	177	192	117	147	NA
	DO (mg/L)	0.5	0.6	0.6	0.6	0.5	NA
	TDS (g/L)	0.115	0.12	0.118	0.156	0.185	NA
	Temp (° C)	20.9	19.5	19.8	18.2	19.2	NA
	Water level (m)[d]	-0.89	-1.26	-1.36	-1.55	-1.64	NA
Radiochemistry (activity in Bq/L)[e]	**^{241}Am (UF)**[f]	15.68 ± 0.38	22.85 ± 0.58	22.09 ± 0.55	25.4 ± 0.64	27.8 ± 1.49	NA
	^{241}Am (F)[g]	7.17 ± 0.19	11.24 ± 0.48	12.15 ± 0.22	21.56 ± 0.59	24.71 ± 1.3	NA
	$^{239+240}$Pu (UF)[f]	30.44 ± 0.9	40.53 ± 1.22	41.71 ± 1.29	43.66 ± 1.27	45.6 ± 2.43	NA
	$^{239+240}$Pu (F)[g]	6.46 ± 0.21	16.28 ± 0.51	17.73 ± 0.56	35.11 ± 0.99	26.93 ± 2.36	NA
Chemistry	**DOC (mg/L)**	4.07	4.15	5.30	5.91	6.77	0.04
	Fe(II) (mM)	0.34	0.39	0.45	0.75	0.92	<0.01
	Fe (mM)	0.42	0.45	0.46	0.80	0.99	<0.01
	Na (mM)	0.73	0.70	0.70	0.79	0.85	<0.01
	SiO_2 (mM)	0.36	0.37	0.37	0.44	0.52	<0.01
	Cl^- (mM)	0.51	0.51	0.51	0.54	0.54	0.01
	Mg (mM)	0.08	0.08	0.08	0.11	0.12	<0.01
	Ca (μM)	33.43	30.69	34.18	41.42	50.40	0.25
	K (μM)	31.71	32.48	32.74	31.97	32.23	0.31
	Mn (μM)	1.80	1.86	1.64	2.00	2.55	<0.02
	P (μM)	4.20	4.20	5.17	7.10	9.69	<1.6
	S (μM)	62.36	62.36	59.25	28.06	6.24	<3.11
	F^- (μM)	2.63	2.11	2.11	3.16	4.21	<0.53
	Br^- (μM)	2.63	2.50	2.50	3.25	4.01	<0.13
	I^- (μM)	4.96	4.81	5.12	7.88	11.03	<0.22
	NO_3^- (μM)	0.24	0.24	0.55	0.00	0.00	<0.01

[a]: day count from the first day with no precipitation after the rainfall event.
[b]: highest concentrations measured on multiple blanks (n > 5) processed in parallel with trench samples
[c]: corrected values against Standard Hydrogen Electrode.
[d]: depth below ground surface.
[e]: plus-minus one standard deviation.
[f]: filtered through 0.45 μm filter (soluble/colloidal).
[g]: unfiltered (total).

Figure captions

Figure 1. pH and E_h (Standard Hydrogen Electrode corrected) measurements from the trench water across the sampling period.

Figure 2. Concentration of elements/ions in the trench water. Bars show the measurements at day 0, 4, 6, 21 and 47 for each element/ion.

Figure 3. Activity of filtered and unfiltered radionuclides measured in the trench water. Filtered fractions (<0.45 µm) are equivalent to soluble and smaller colloidal particles. Unfiltered fractions are as considered total concentrations. Error bars show the standard deviation of triplicate measurements.

Figure 4. Taxa relative abundances over time. Only taxa with an average relative abundance >5% of the total sequences in at least a single sampling day are shown. Taxa with <5% of all sequences are grouped under 'other'. Phyla with <5% of relative abundance at all times are grouped under 'other phyla', except Archaea.

Figure 5. Changes in the relative abundances of selected RXNs over time. A, Cytochrome C oxidase; B, cellulase; C, malate synthase; D, 5-methyltetrahydrosarcinapterin:corrinoid/iron-sulfur protein *Co*-methyltransferase (CH_3-HSPT:Fe-S protein *Co*-MT); E: sulfite reductase; and F, superoxide dismutase.

Figure 6. Global scheme of the processes at LFLS. Orange details on barrels reading Fe^{3+} represent solid Fe^{3+} minerals, mainly (oxy)hydroxides. Colour of arrows represent the time at which each process takes place: red, aerobic/after rain; brown, microaerophilic; blue, anaerobic/dry phase; and black arrows indicate processes that seem to be independent from the sampling time. Dashed arrows indicate transport. Abbreviations used in the figure: C_{org}, organic carbon; MIC, microbially induced corrosion.

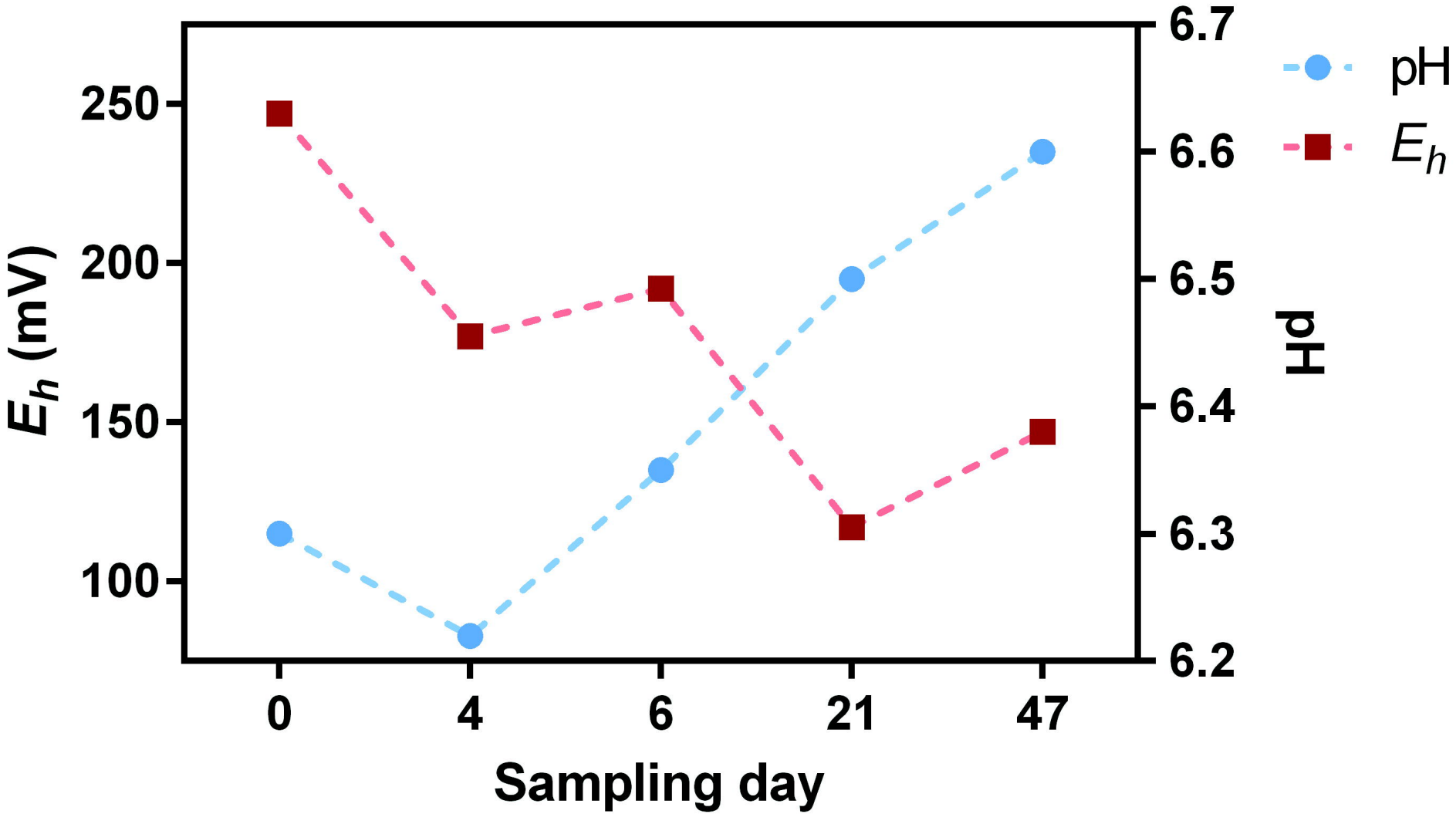
250
200
150
100
E_h (mV)
6.7
6.6
6.5
6.4
6.3
6.2
pH
0
4
6
21
47
Sampling day
pH
E_h

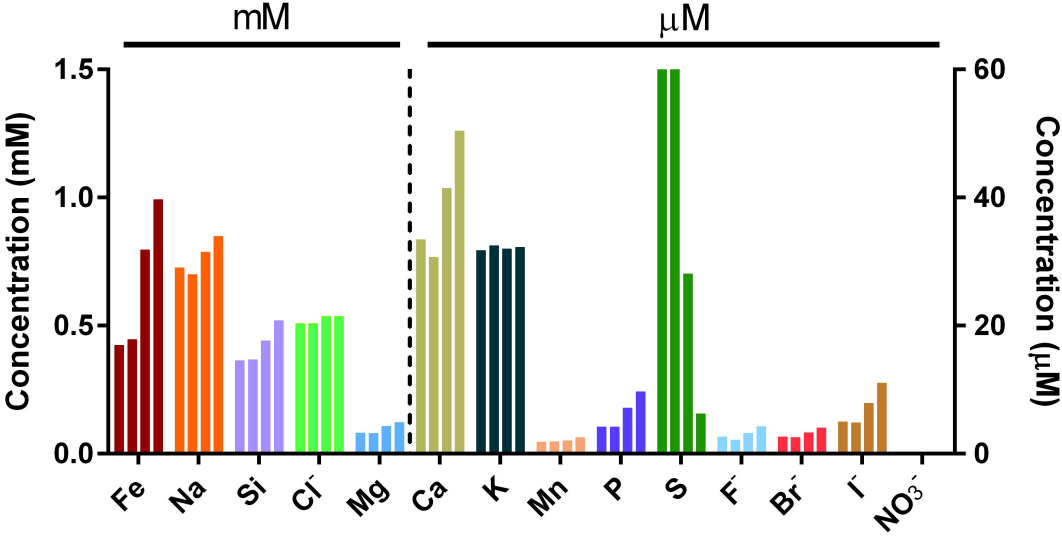
mM
μM
Concentration (mM)
Concentration (μM)
1.5
1.0
0.5
0.0
60
40
20
0
Fe
Na
Si
Cl⁻
Mg
Ca
K
Mn
P
S
F⁻
Br⁻
I⁻
NO3⁻

Figure 3

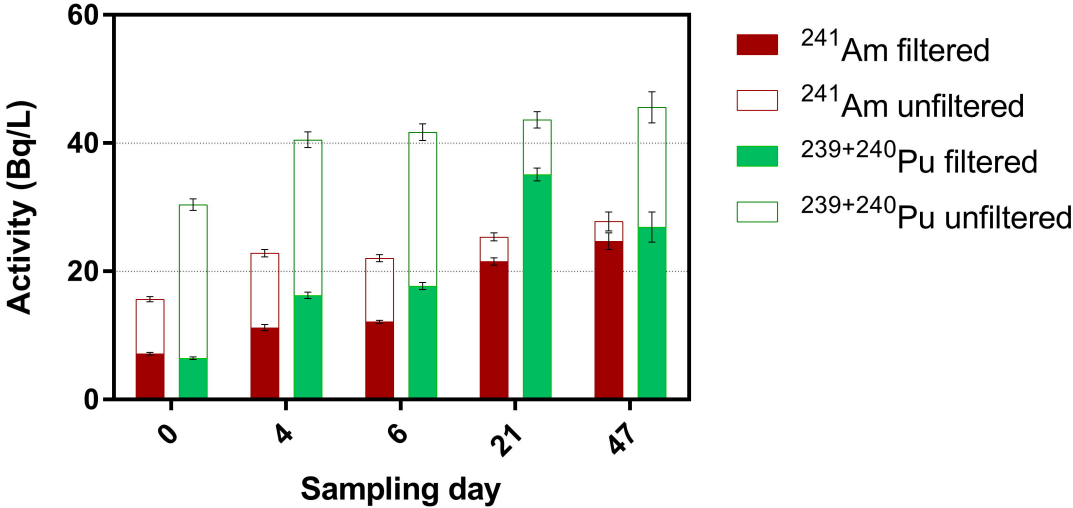
60
40
20
0
Activity (Bq/L)
0
4
6
21
47
Sampling day
241Am filtered
241Am unfiltered
239+240Pu filtered
239+240Pu unfiltered

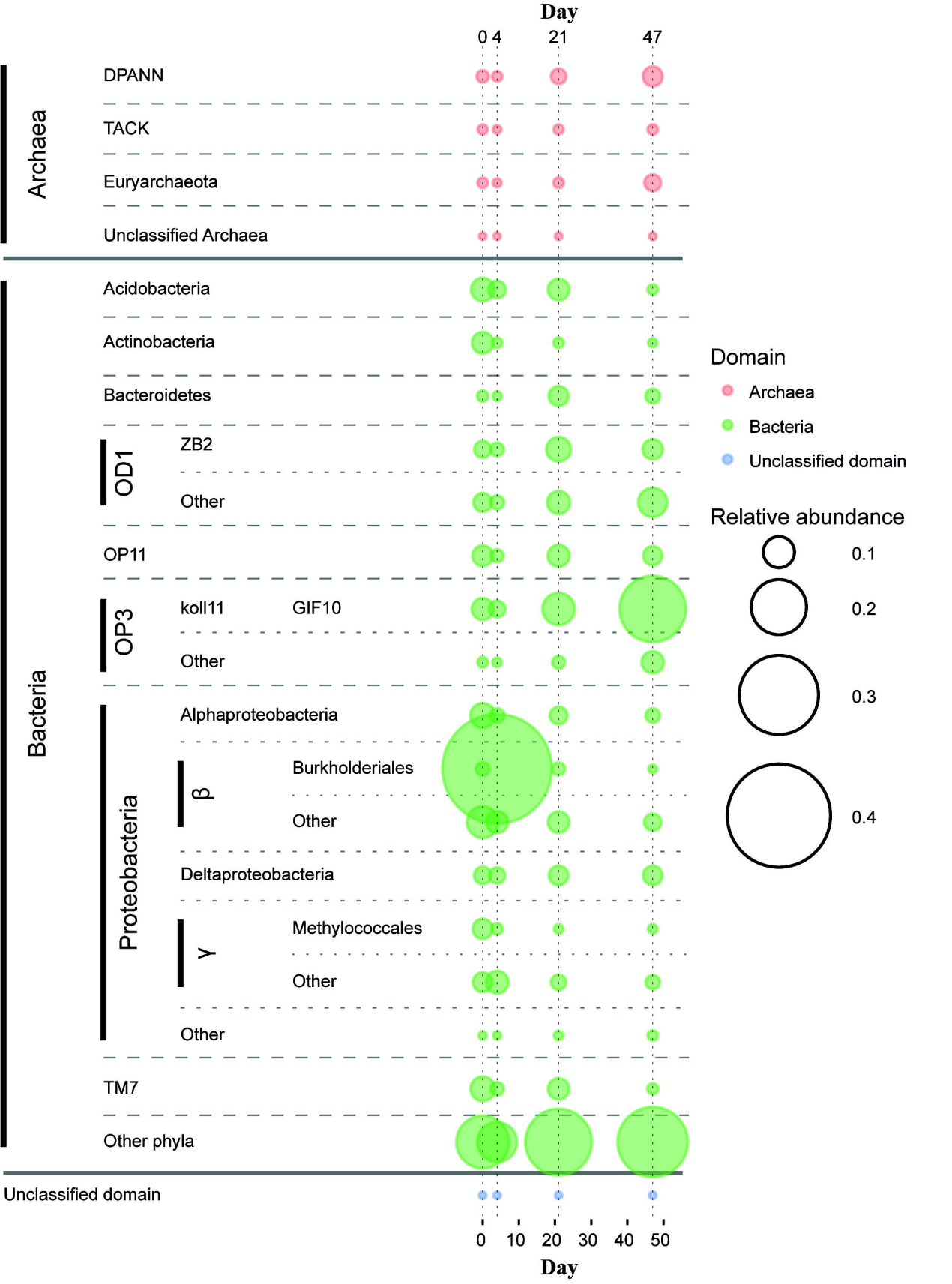
Day
0 4
21
47
Archaea
DPANN
TACK
Euryarchaeota
Unclassified Archaea
Bacteria
Acidobacteria
Actinobacteria
Bacteroidetes
OD1
ZB2
Other
OP11
OP3
koll11
GIF10
Other
Proteobacteria
Alphaproteobacteria
β
Burkholderiales
Other
Deltaproteobacteria
γ
Methylococcales
Other
Other
TM7
Other phyla
Unclassified domain
0 10 20 30 40 50
Day
Domain
Archaea
Bacteria
Unclassified domain
Relative abundance
0.1
0.2
0.3
0.4

Figure 5

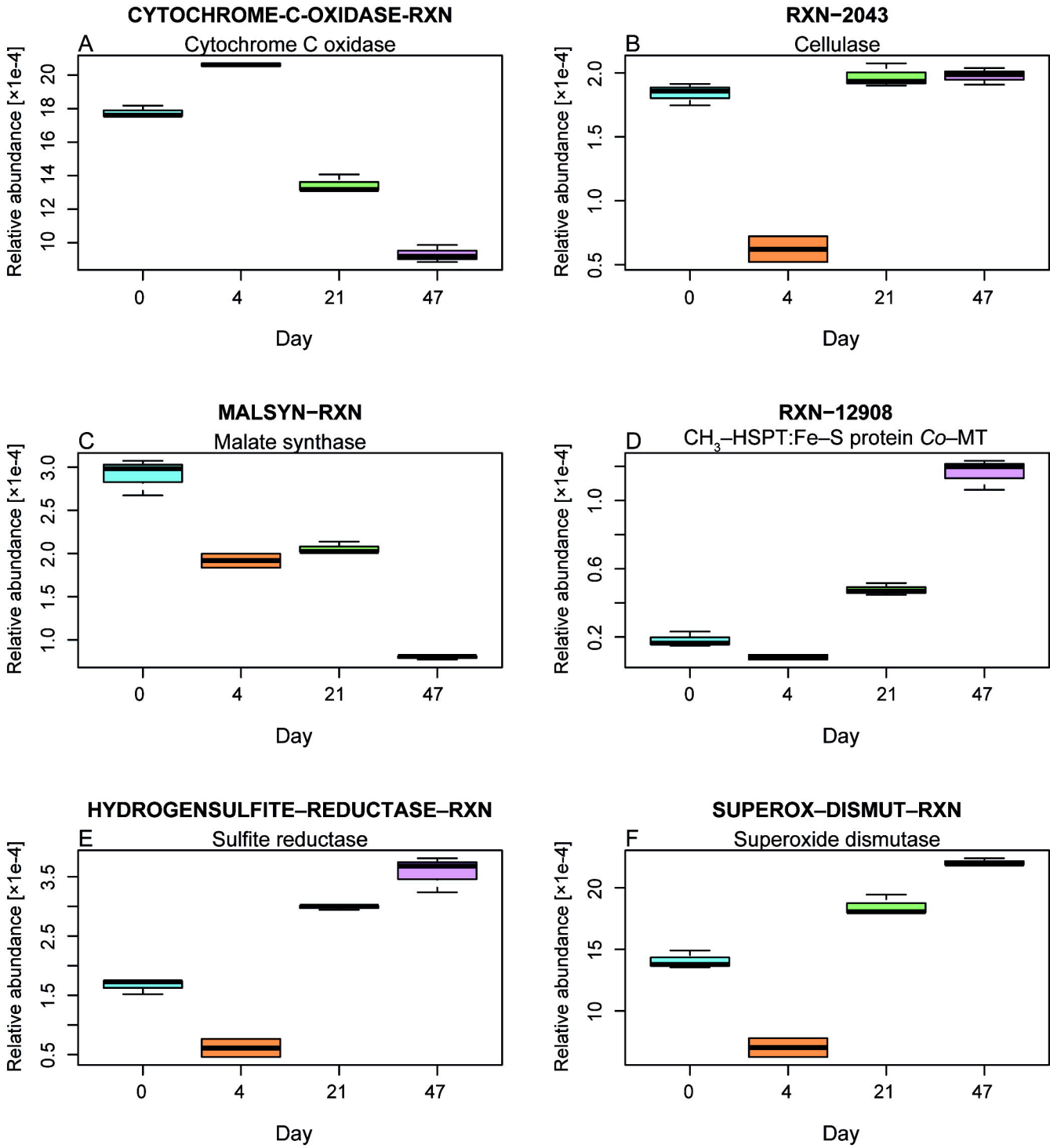
CYTOCHROME-C-OXIDASE-RXN
A
Cytochrome C oxidase
Relative abundance [×1e-4]
10 12 14 16 18 20
0 4 21 47
Day
RXN−2043
B
Cellulase
Relative abundance [×1e-4]
0.5 1.0 1.5 2.0
0 4 21 47
Day
MALSYN−RXN
C
Malate synthase
Relative abundance [×1e-4]
1.0 1.5 2.0 2.5 3.0
0 4 21 47
Day
RXN−12908
D
CH3–HSPT:Fe–S protein Co–MT
Relative abundance [×1e-4]
0.2 0.6 1.0
0 4 21 47
Day
HYDROGENSULFITE–REDUCTASE–RXN
E
Sulfite reductase
Relative abundance [×1e-4]
0.5 1.5 2.5 3.5
0 4 21 47
Day
SUPEROX–DISMUT–RXN
F
Superoxide dismutase
Relative abundance [×1e-4]
10 15 20
0 4 21 47
Day

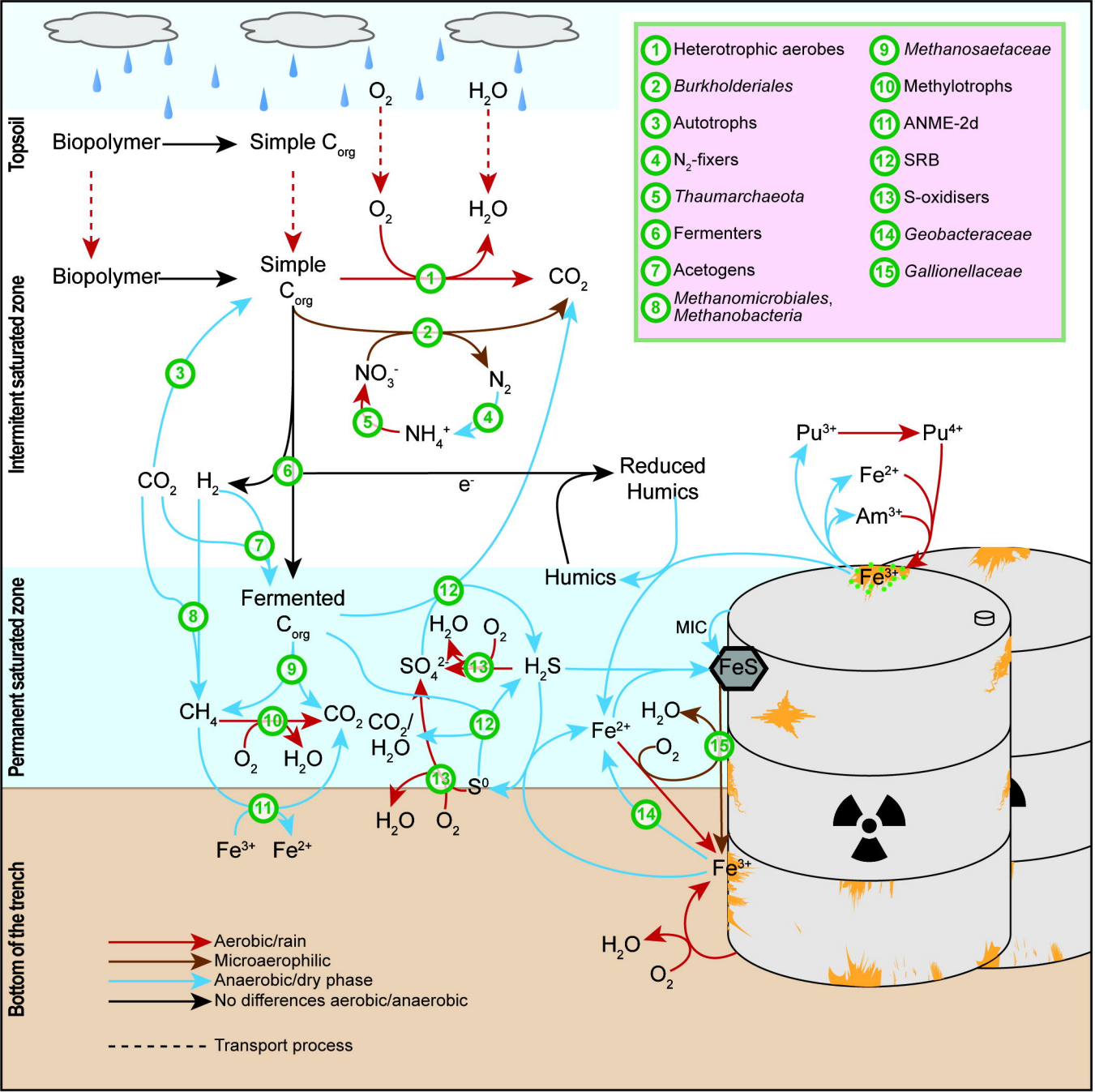
Topsoil
Intermitent saturated zone
Permanent saturated zone
Bottom of the trench
Biopolymer
Simple C_{org}
O_2
H_2O
Biopolymer
Simple C_{org}
CO_2
NO_3^-
N_2
NH_4^+
CO_2
H_2
e^-
Reduced Humics
Humics
Fermented C_{org}
CH_4
CO_2
O_2
H_2O
CO_2/ H_2O
SO_4^{2-}
H_2S
S^0
Fe^{3+}
Fe^{2+}
Pu^{3+}
Pu^{4+}
Am^{3+}
MIC
FeS
Aerobic/rain
Microaerophilic
Anaerobic/dry phase
No differences aerobic/anaerobic
Transport process
1 Heterotrophic aerobes
2 Burkholderiales
3 Autotrophs
4 N_2-fixers
5 Thaumarchaeota
6 Fermenters
7 Acetogens
8 Methanomicrobiales, Methanobacteria
9 Methanosaetaceae
10 Methylotrophs
11 ANME-2d
12 SRB
13 S-oxidisers
14 Geobacteraceae
15 Gallionellaceae